FINITE ELEMENT MODEL UPDATE OF A VERY FLEXIBLE FLYING WING USING GROUND VIBRATION TESTING DATA

Bilal Sharqi[1] and Carlos E. S. Cesnik[1]

[1]University of Michigan
Ann Arbor, Michigan 48109 USA
Postdoctoral Fellow, bilalsh@umich.edu
Richard A. Auhll Department Chair, Clarence L. "Kelly" Johnson Collegiate Professor of Aerospace Engineering, cesnik@umich.edu

Abstract: Ground vibration testing is typically conducted on an aircraft where the structure is supported using a suspension setup that emulates the free-flying aircraft. When the structure is very flexible, it is challenging to find a suspension system that can support the structure without influencing its dynamic response. This study investigates the computational and experimental techniques required to conduct such a GVT on a very flexible aircraft and update its finite element model. The two main challenges associated with conducting GVT on a VFA are the measurement of the low frequencies (< 1.0 Hz) related to the test structure and the practical challenge of obtaining a suspension that is soft enough to minimize the interaction between the suspension modes and the elastic modes of the aircraft. For VFA, decoupling of the suspension and airframe modes is typically not feasible. This requires accounting for the suspension in the FEM, which can be achieved by characterizing the suspension upfront as an isolated component and accounting for it in the FEM. This work details the process of performing GVT on a VFA with the suspension model included and removing it once the FEM is successfully updated. This results in a FEM that is dynamically representative of the actual test structure, bypassing the need for an expensive and potentially impractical free-free GVT.

1 INTRODUCTION

During ground vibration testing (GVT) [1–4], the way an aircraft is supported determines its boundary conditions [5, 6]. In order to simulate the real aircraft in flight, the support needs to be as close as possible to the free-flying condition. In reality, a truly free boundary condition is an oxymoron. If there is a boundary condition, there will be something external to the aircraft connected to it that will impact the response of the structure under excitation [7]. Ideally, the natural frequency associated with the support system should be separated from the lowest elastic frequency of the test structure by at least an order of magnitude [8]. While this is already challenging for conventional, rigid aircraft [9], the low stiffness and low fundamental frequency of a very flexible aircraft (VFA) requires a very soft suspension system to get a reasonable separation between the structure and the support mechanism [6]. It can also become challenging to find a suspension/support that has the right stiffness characteristics and can support the test structure without deforming excessively.

VFA can exhibit significantly different deformed shapes when subjected to different loads in flight [10–12]. Being very flexible, they also deform substantially based on boundary conditions in laboratory conditions [13]. This requires testing the aircraft in multiple deformed

configurations representative of in-flight trim shapes to completely characterize its structural dynamics [14]. A variety of numerical studies have been performed demonstrating the variation in shapes of very flexible structures based on suspension location (essentially adjusting the boundary condition) and their impact on the structure [15, 16]. However there is a lack of reported studies experimentally demonstrating the impact of the deformed shapes, the variation in the structure's response based on the shape, and the subsequent finite element model (FEM) update. To obtain an accurate understanding of the structural dynamics of an aircraft, a GVT needs to be conducted with a very soft suspension [17] and address the various challenges associated with designing and performing such an experiment.

FEM updating is a continually improving topic of research as new algorithms and techniques are developed. Ereiz et al. [18] provide a summary of some of the methods currently employed for FEM updating. Sharqi and Cesnik [14] developed an FEM updating process with the ability to account for large displacements and geometric nonlinearities to update the FEM of very flexible structures. Recently, Li and Zhang [19] studied the FEM update problem using an unscented Kalman Inversion to solve the FEM update problem in a gradient-free manner.

This work presents a real-life application of a new FEM updating methodology for very flexible structures where their shape can vary significantly in the vicinity of their operating conditions [14]. In order to obtain a sample set of possible deformed shapes the structure can reach within its operating envelope, one can vary the structural support under gravity field imposed onto the structure during GVT [13, 15] or other ways to vary the loads (e.g., as experienced by the structure during maneuvers [20]). This new methodology has been numerically demonstrated on a built-up FEM of very flexible wing structures in past work [14] and then applied to update the FEM of experimental test cases [21].

This paper focuses on the application and validation of GVT and the FEM updating methodologies on a very flexible aircraft, the X-HALE. Being very flexible and made of lightweight composite materials, the airframe presents the ideal structure to exercise all the developments and findings from past work [13]. Section 2 discusses the methodology used for GVT and FEM updating on the VFA while Section 3 discusses the characteristics of the X-HALE airframe. Section 4.1 provides a summary of the GVT campaign on the aircraft. Section 4.2 discusses the application and results of the finite element model updating methodology on the VFA, while Section 4.3 presents the validation of the methodologies through a free-free GVT on the X-HALE. Section 5 summarizes the work done and outlines the future work that will be conducted towards improving GVT and FEM updating techniques for very flexible structures.

2 METHODOLOGY

2.1 Ground Vibration Testing

While GVT of moderately flexible aircraft can be conducted in a single, undeformed (jig) shape, a single-point characterization (for a given mass condition) may not be sufficient to calibrate the FEM of a VFA, as shown in [14]. Indeed, VFA achieve different configurations during normal operations, and these configurations are significantly different from the undeformed shape on the ground. The effects of these geometry changes need to be accounted for and characterized by testing the aircraft in different deformed shapes that can be achieved, for instance, by means of multiple suspension points placed at variable locations along the span. However, if variable or multiple suspension points are used, the effect of each suspension point needs to be individually characterized and identified. The process is shown schematically in Fig. 1.

This study uses a methodology for GVT on very flexible structures that addresses the above challenges [13]. A low-frequency elastic support suitable for suspending the structure is designed and built using a series of springs in a laboratory setting. The support is characterized and included in the FEM of a VFA test case. The numerical models are used to test various suspension configurations (or deformed shapes) using the experimentally identified suspension setup characteristics. Moreover, the FEMs are also used to investigate the support system's influence on the modal parameters of the support-structure assembly. Once GVT results were available, the test structure's FEM was updated (as shown in Section 4.2.3) to match the measured structural modal parameters while keeping the FEM of the support system unchanged. Since the support system is characterized upfront as an isolated component, this results in a correct updating of the FEM such that it is dynamically representative of the actual test structure.
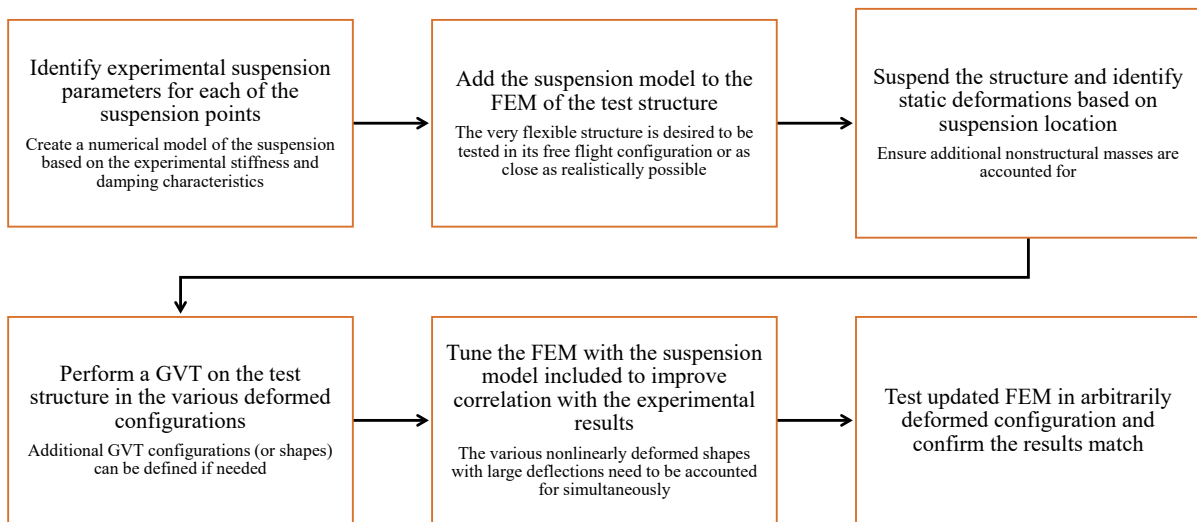

Figure 1: Algorithm for GVT and FEM updating of very flexible structures.

2.2 Finite Element Model Updating

When updating the FEM of a structure, a common first step is to check the stiffness model through a static test validation and updating process. In the case of very flexible structures, loads causing large displacements may also change the mass properties and would be needed for the subsequent vibration (modal analysis) test used to update the mass model. However, in the scope of this work, the objective was to apply the most generic FEM updating process (adapted for very flexible structures) that can handle both the mass and stiffness design variables. There can be multiple variations of the problem setup, *e.g.,* one can tune the stiffness model first using multiple deformed cases and then tune the mass model under the same load cases. However, these variations on the problem setup are not studied as part of this work. The typical FEM updating process is shown schematically in Fig. 2.

The FEM updating problem for VFA can be cast as an optimization problem subjected to multiple nonlinear static shapes about which linearized results are obtained and compared against the GVT data [14]. The methodology for updating the FEM of VFA is shown schematically in Fig. 3. In this process, the updated FEM obtained from the optimization process is tested against a new set of GVT results generated within the bounds of deformation used for calibration. If
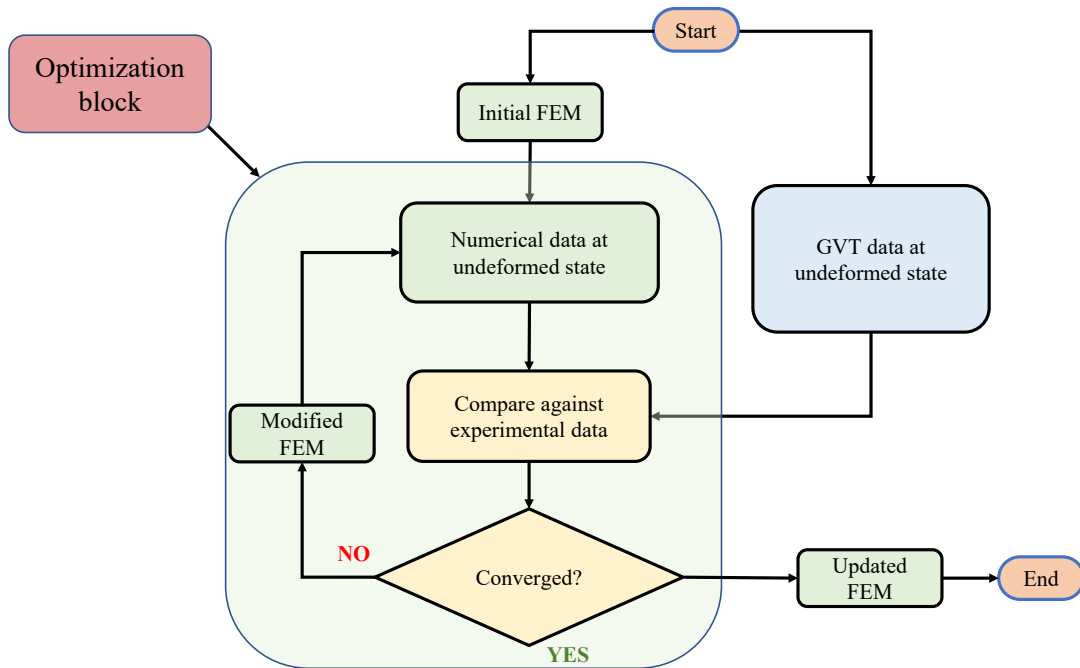
Figure 2: Typical finite element model updating process.

the updated FEM can capture the results of the new load case within predefined tolerances, the updated FEM is retained, and the updating process concluded. If the results do not match, additional GVT data under different deformed shapes are needed. During GVT, moving the point of suspension affects the shape as well as the modal parameters in a similar manner as in-flight loads for a VFA. Additionally, there is the impact of the suspension itself. The FEM updating process was augmented to handle multiple deformed configurations simultaneously resulting from different boundary conditions coming from different suspension configurations (as opposed to the deformations coming from a load factor), along with the suspension effects.
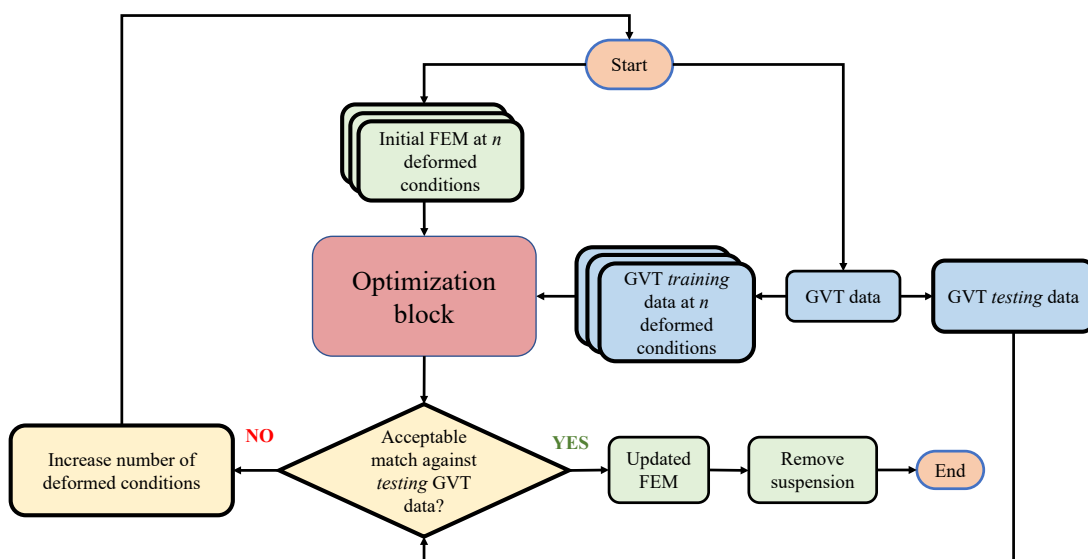

Figure 3: Modified process for FEM updating for very flexible structures.

The optimization problem used in the FEM updating process is written as:

$$
\begin{aligned}
\textbf{minimize F(x)} \quad = \quad & \left(\frac{m - m_0}{m_0}\right)^2 + \left(\frac{I_{xx} - I_{xx_0}}{I_{xx_0}}\right)^2 + \left(\frac{I_{yy} - I_{yy_0}}{I_{yy_0}}\right)^2 + \left(\frac{I_{zz} - I_{zz_0}}{I_{zz_0}}\right)^2 + \\
& \left(\frac{X_{cg} - X_{cg_0}}{X_{cg_0}}\right)^2 + \left(\frac{Y_{cg} - Y_{cg_0}}{Y_{cg_0}}\right)^2 + \left(\frac{Z_{cg} - Z_{cg_0}}{Z_{cg_0}}\right)^2 + \\
& \sum_{j=1}^{n} \sum_{i=1}^{N} \left(\frac{\omega_i^j - \omega_{i_0}^j}{\omega_{i_0}^j}\right)^2
\end{aligned}
$$

$$
\begin{aligned}
\textbf{with respect to:} \quad & \mathbf{x} \\
\textbf{subjected to:} \quad & m^\ell \leq m \leq m^u \\
& I_{xx}^\ell \leq I_{xx} \leq I_{xx}^u \\
& I_{yy}^\ell \leq I_{yy} \leq I_{yy}^u \\
& I_{zz}^\ell \leq I_{zz} \leq I_{zz}^u \\
& X_{CG}^\ell \leq X_{CG} \leq X_{CG}^u \\
& Y_{CG}^\ell \leq Y_{CG} \leq Y_{CG}^u \\
& Z_{CG}^\ell \leq Z_{CG} \leq Z_{CG}^u \\
& MAC_i^j \geq MAC_{min}; \quad i = 1, 2, ..., N \quad \text{and} \quad j = 1, 2, ..., n \\
& \mathbf{x}^\ell \leq \mathbf{x} \leq \mathbf{x^u}
\end{aligned}
\tag{1}
$$

where index $i = 1, \ldots, N$ represents the modal number for the first N modes for each of the jth deformed shape associated with the set of n shapes. The terms with the subscript o refer to the experimental value while the terms without the subscript are the corresponding numerical components. Furthermore, m is the total mass of the structure, X_{cg} through Z_{cg} refers to the three components of the center of gravity (c.g.) location, while I_{xx} through I_{zz} are the components of the inertia tensor (additional components of the inertia tensor can also be included, but are not shown or investigated here for brevity); ω_i^j is the ith natural frequency associated with the jth deformed shape. Finally, MAC stands for Modal Assurance Criterion [22], and MAC_{min} corresponds to the desired minimum threshold of acceptable modal correlation. The upper and lower bounds in the constraints are denoted by the superscripts u and ℓ, respectively.

3 X-HALE TESTBED

The University of Michigan's X-HALE is an experimental testbed for identifying areas of improvement needed in design, analysis and control of VFA [20]. The X-HALE was designed to:

1. be aeroelastically representative of a HALE aircraft and exhibit nonlinear couplings between flight dynamics and structural dynamics;
2. be capable of large static deflections, with a tip deflection greater than 30% of the semi-span during operation;
3. enable studying control design methodologies for VFA.

The X-HALE is a very flexible, remote-piloted aircraft developed with the primary objective of collecting experimental aeroelastic data and serving as a platform to evaluate control strategies.

It is a wing-boom-tail type of aircraft with a 6-meter span, divided into six sections of 1-meter long each, with the tip sections set at a dihedral angle of 10 deg. The wing has an EMX-07 airfoil profile with chord length of 0.2 m, while the tails have a NACA 0012 airfoil profile with chord length of 0.12 m. There are 11 control effectors available on board the VFA: two roll spoilers located at the dihedral sections, four elevators, one at each outboard tail, and five motors providing distributed electric propulsion. The center tail is not used as a control surface.

The configuration is being experimentally studied both on the ground (GVT [13] – discussed here) and in flight [12]. These tests are building up a unique set of coupled nonlinear aeroelastic-flight dynamics data to support validation of numerical modeling, analysis and simulation tools. The X-HALE configuration can be seen both on the ground and in flight in Fig. 4, highlighting the level of deformation attained by the aircraft in flight. Its main physical characteristics are listed in Table 1.

Figure 4: X-HALE airframe on the ground and in flight.

Table 1: Main X-HALE airframe characteristics.

Wing span	6	m
Wing chord	0.2	m
Planform area	1.2	m^2
Aspect ratio	30	-
Propeller diameter	0.3	m
Gross take-off weight	11.35	kg

4 APPLICATION OF GVT AND FEM UPDATING METHODOLOGIES ON VFA

This section focuses on the application of the GVT and the FEM updating methodologies on X-HALE. GVT was performed on the airframe in multiple deformed configurations using both an impact hammer and a shaker as excitation sources. Prior to the GVT, the suspension system was characterized and included in the FEM, according to the methodology mentioned in 2.1. A moderately stiff spring with a spring constant of 195 N/m was selected for the laboratory GVT and ten such springs were used in series for each side of the suspension (for a net stiffness value of 19.5 N/m per set of springs). Since the total extension experienced by the ten springs is greater than the vertical height of the test rig, a single low-friction, ball-bearing pulley was used to allow the springs to extend horizontally along the length of the test rig and then turn directions (to drop vertically) in order to suspend the X-HALE. Once the experimental GVT data was collected, the FEM updating process was implemented based on the process shown in Section 2.2.

4.1 GVT Results

For the GVT on the X-HALE, the following configurations were defined:

1. X-HALE suspended from the outboard wing junctions, shown in green in Fig. 5 (the joints between the outermost wings and the ones adjacent to it)
2. X-HALE suspended from the inboard wing junctions, shown in red in Fig. 5 (the joints between the wings at center and 1 m away from the center).
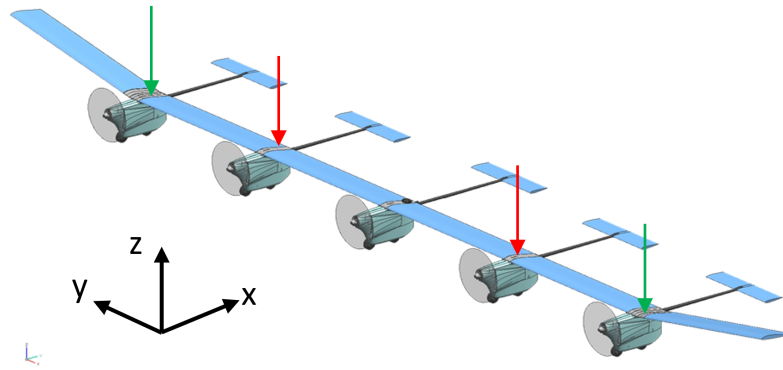

Figure 5: X-HALE configurations for GVT based on suspension location. Red and green arrows represent inboard and outboard suspensions respectively.

These two configurations are defined because the joint between the wings is a connection point from which the aircraft can be suspended. Moreover, using a combination of the two suspension configurations allows to recover most of the vehicle in-flight shapes. These two suspension configurations are at the extremes of the deformations the aircraft normally experiences in flight.

The aircraft setup in the laboratory during GVT for the outboard configuration is shown in Fig. 6. The X-HALE setup in the inboard configuration is shown in Fig. 7. The suspension system consisting of a series of springs and a pulley to turn directions can be seen above the aircraft.
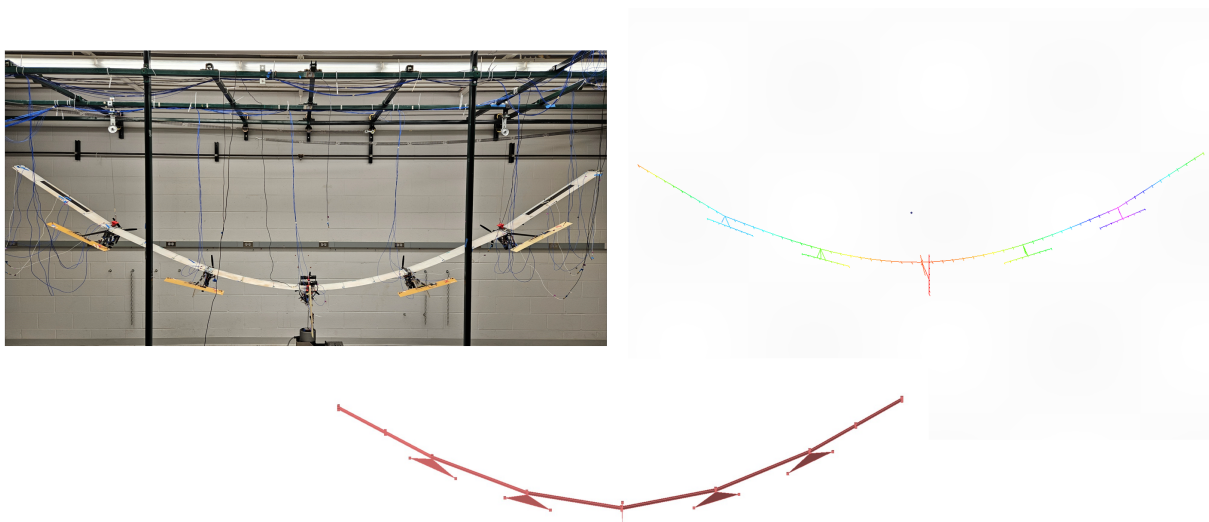

Figure 6: The X-HALE setup for GVT in the outboard configuration (top left), the corresponding nonlinear model of the static deformed shape under self weight (top right), and the reference shape used in the test software to define the initial geometry based on the accelerometer layout (bottom).
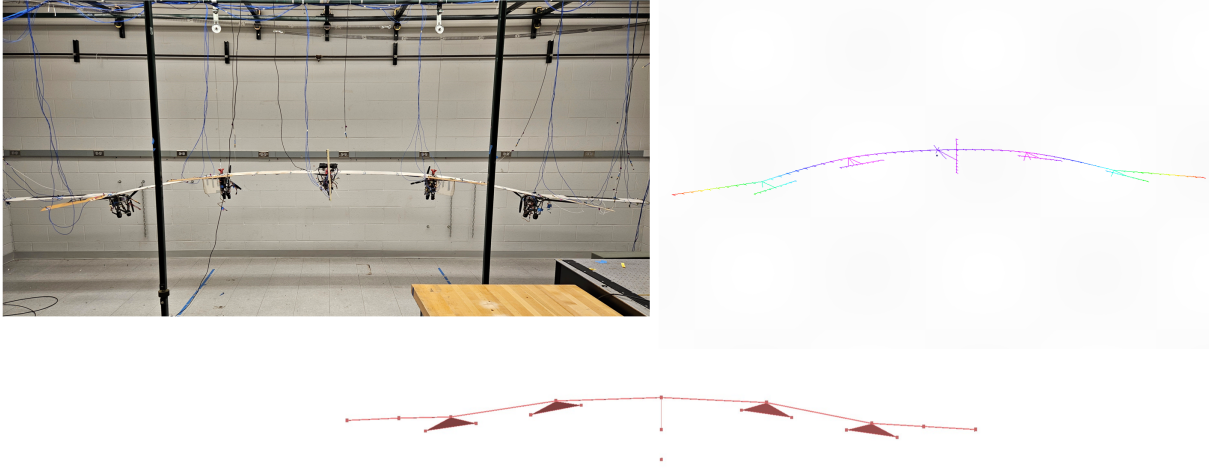
Figure 7: The X-HALE setup for GVT in the inboard configuration (top left), the corresponding nonlinear model of the static deformed shape under self weight (top right), and the reference shape used in the test software to define the initial geometry based on the accelerometer layout (bottom).

The results from laboratory GVT performed with both the shaker and impact hammer as excitation sources, compared against the FEM are summarized in Figs. 8 and 9 for the outboard and inboard configurations respectively. They indicate that while the experimental results show good agreement between themselves, there are large errors of up to 15% between the initial FEM and the GVT. The different configurations also exhibit notable differences between each other, shown in Fig. 10. These results highlight the need to update the FEM of the X-HALE considering both the configurations simultaneously, and the process is discussed in the following sections.

4.2 FEM Updating on the X-HALE

During GVT of the X-HALE, the deformed shape for the structure was achieved by changing the location of the suspension. In this case, the gravitational loading (self-weight) for the very flexible structure causes the deformation. However, the placement of the suspension (i.e., boundary conditions applied to the structure) affect the loading and therefore the deformed shape. In the FEM updating process described in past work [14], the deformed shapes were obtained purely from changing the inertial loads acting on the structure and not by adjusting the suspension location (or boundary conditions). Moving the point of suspension affects the shape as well as the modal parameters in a similar manner as the loads being applied. The FEM updating process was augmented to simultaneously handle multiple deformed configurations resulting from different boundary conditions (as opposed to the deformations coming from a load factor applied to the gravitational loading). The optimization framework developed as part of this work was used to update the FEM of the X-HALE as it undergoes large deformations under gravitational loading, as a result of the different boundary conditions applied during suspension.

4.2.1 Problem setup

The FEM updating process developed in [14] and shown schematically in Fig. 3 was used to set up the FEM updating problem for the X-HALE. The GVT training data used came from the impact GVT conducted on the airframe in the outboard and the inboard configurations. The input file provided to the nonlinear structural and modal solver (Nastran's SOL400) to run the subcases corresponding to different configurations required creating a set up where for one
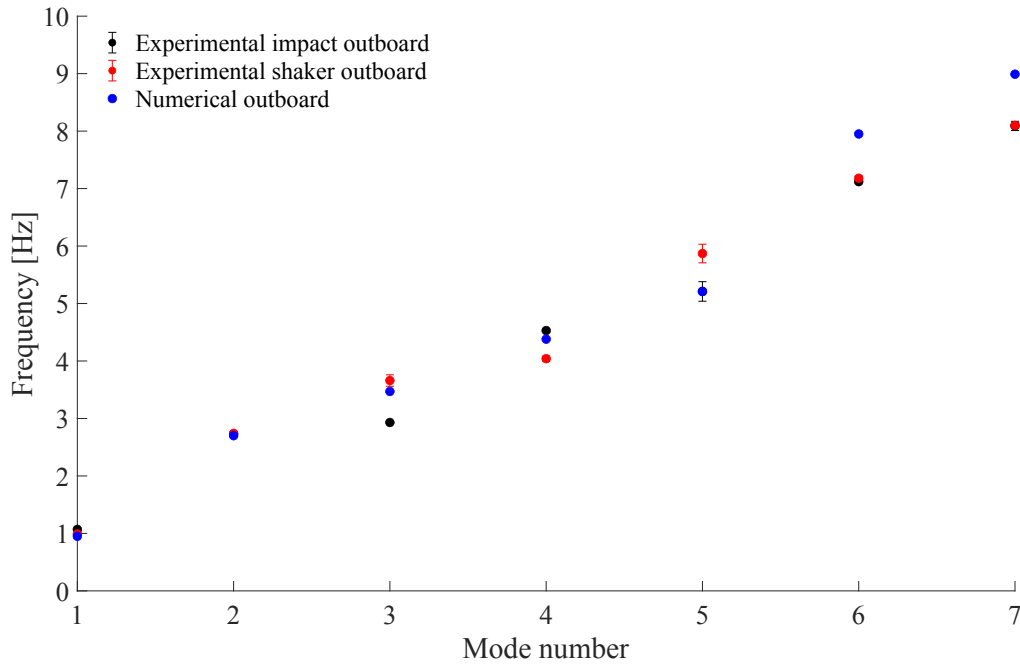
Figure 8: Comparison of the first 7 modes from the shaker and impact hammer GVT vs. the initial FEM for the outboard configuration.
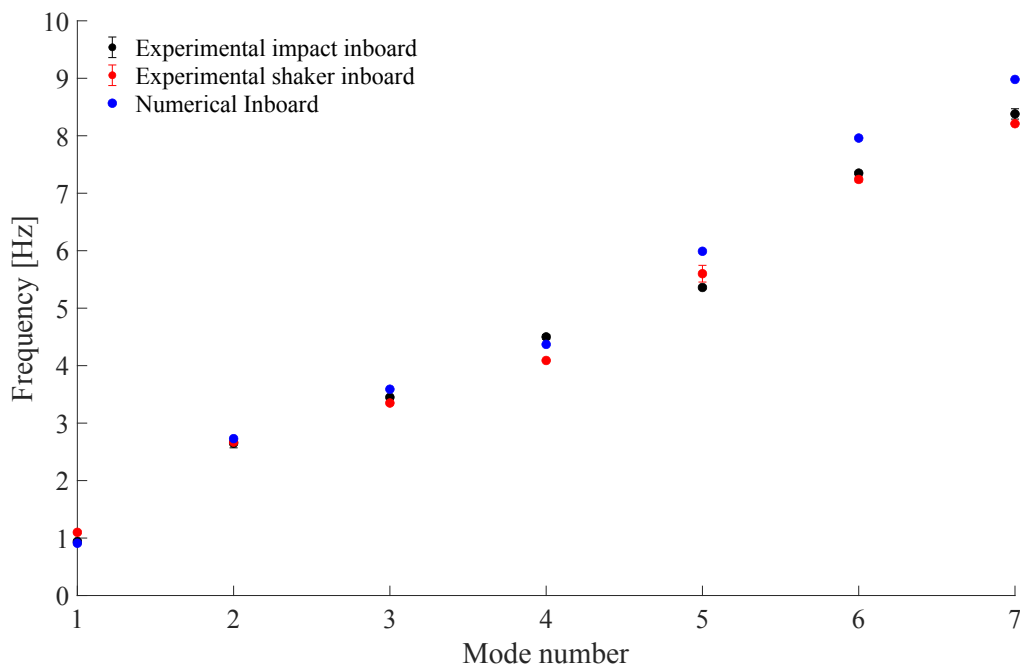

Figure 9: Comparison of the first 7 modes from the shaker and impact hammer GVT vs. the initial FEM for the inboard configuration.

subcase, the set of boundary conditions pertaining to the outboard configuration would be active. For the other subcase, the set of boundary conditions pertaining to the inboard configuration would be active.
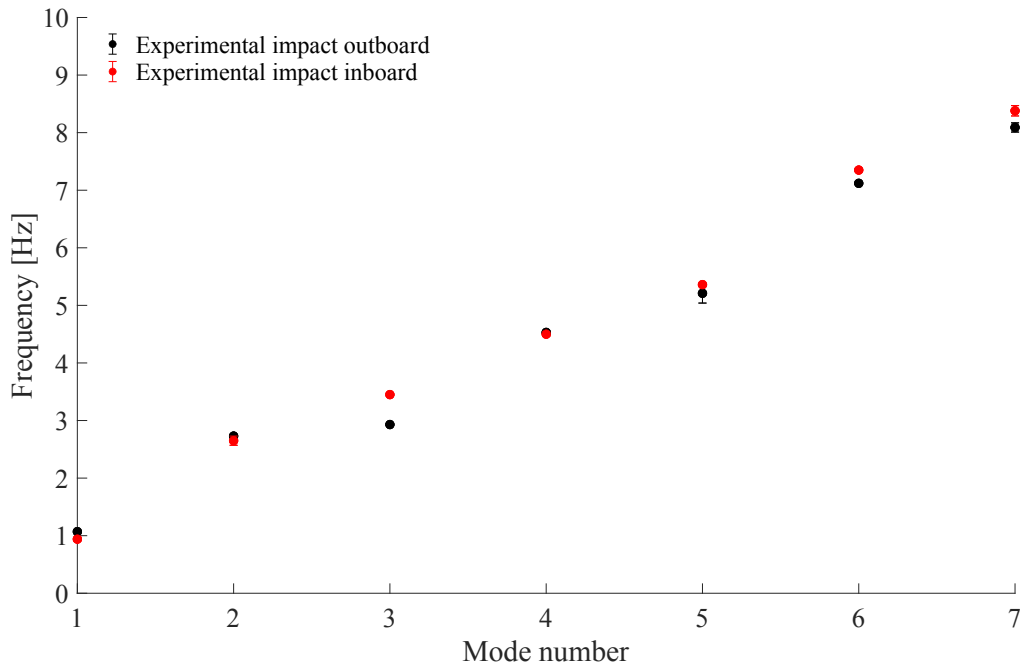
Figure 10: Comparison of the first 7 modes from the outboard vs. inboard impact hammer GVT.

4.2.2 Design Variables, Bounds, and Constraints

Material properties of the different wings and joiners (the pieces that connect two wings) were chosen as design variables for the X-HALE. Originally, the material properties were defined as constant along the entire structure for all the wings and joiners, but that is not representative of the actual construction. Different wing segments were constructed at different times and have been used differently (i.e., damaged wings have been repaired or replaced after flight tests). This leads to the wings having noticeable differences between their sitffnesses - including differing tension on the skin. The joiners currently on the airframe were not manufactured in the same batch and have different wall thicknesses, which causes their stiffness to be variable between wing junctions. No attempt was made to individually characterize each component, since there are too many unknowns affecting their response. Design variables pertaining to these components were allowed larger bounds, which will allow for identifying and fine tuning the differences between the different segments as well as the nonlinearities that come from the junction or the segment interfaces (some of the components are glued together and represent an imperfect contact patch, while some other have Aluminum brackets connecting different components and are fastened by hand).

Inequality constraints are imposed on the total mass, inertia and center of gravity properties. The design variables had variable bounds placed on them based on the level of uncertainty on their original values. The mass or density related design variables have the tightest bounds since the mass of individual components and the entire structure can be measured. The bounds on the wing and joiner related design variables were wider since the age, connection imperfectness and manufacturing tolerances create both nonlinearities and uncertainties. The bounds on the design variables related to the wing and tail connections were the most relaxed (widest) since those material properties are the least certain. The constraint variables had upper and lower limits set within $\pm 10\%$ of their original values.

The design variables chosen for the optimization problem are shown in Table 2, along with their values before and after the updating process. Here, WR1 refers to the first wing to the right of the center of the X-HALE, while WL1 refers to the first wing to the left. Similarly WR2 and WL2 refer to the second wings to the right and left of the center respectively. The joiners are machined pieces milled out of Aluminum stock that connect two wings to each other, and their naming reflects the two wings they connect to. The tail boom is the relatively rigid rod that connects the pitch elevators to the wings. The Wing-Tail spring refers to the spring that is used to model the connection between the tail boom and the wing. On the X-HALE, the wing-tail connection is accomplished by sliding the tail boom onto a tail boom connector. This connector is fastened to the pods attached at each wing junction. The tail boom is not screwed in, but after sliding on to the connector, is held into place by using metal tape to wrap around the end of the boom and the adapter installed on the wing. This connection presents a large uncertainty (or bounds in an optimization problem) during the FEM creation and updating process.

Table 2: Design variables (DV) for the FEM update of the X-HALE using laboratory GVT results.

DV Type	Component	Normalized bounds	Initial DV	Final DV	Units	Difference (vs. initial) %
Young's Modulus	WR3	0.75, 1.25	4.32	5.02	GPa	16.3
Young's Modulus	WR2	0.75, 1.25	4.32	3.57	GPa	17.4
Young's Modulus	WR1	0.75, 1.25	4.32	4.51	GPa	4.5
Young's Modulus	WL1	0.75, 1.25	4.32	4.94	GPa	14.5
Young's Modulus	WL2	0.75, 1.25	4.32	3.78	GPa	12.5
Young's Modulus	WL3	0.75, 1.25	4.32	3.28	GPa	24.0
Young's Modulus	WL1-WR1 joiner	0.75, 1.25	4.32	4.64	GPa	7.5
Young's Modulus	WR1-WR2 joiner	0.75, 1.25	4.32	4.33	GPa	0.4
Young's Modulus	WL1-WL2 joiner	0.75, 1.25	4.32	4.41	GPa	2.1
Young's Modulus	WR2-WR3 joiner	0.75, 1.25	4.32	4.06	GPa	5.9
Young's Modulus	WL2-WL3 joiner	0.75, 1.25	4.32	4.17	GPa	3.4
Young's Modulus	Tail Boom	0.75, 1.25	5.00	4.99	GPa	0.3
Shear Modulus	WR3	0.75, 1.25	1.71	1.69	GPa	1.1
Shear Modulus	WR2	0.75, 1.25	1.71	1.70	GPa	0.5
Shear Modulus	WR1	0.75, 1.25	1.71	1.75	GPa	2.1
Shear Modulus	WL1	0.75, 1.25	1.71	1.67	GPa	2.1
Shear Modulus	WL2	0.75, 1.25	1.71	1.71	GPa	0.3
Shear Modulus	WL3	0.75, 1.25	1.71	1.79	GPa	4.8
Shear Modulus	WL1-WR1 joiner	0.75, 1.25	1.71	1.72	GPa	0.8
Shear Modulus	WR1-WR2 joiner	0.75, 1.25	1.71	1.76	GPa	2.7
Shear Modulus	WL1-WL2 joiner	0.75, 1.25	1.71	1.77	GPa	3.7
Shear Modulus	WR2-WR3 joiner	0.75, 1.25	1.71	1.78	GPa	3.8
Shear Modulus	WL2-WL3 joiner	0.75, 1.25	1.71	1.77	GPa	3.6
Shear Modulus	Tail Boom	0.75, 1.25	1.88	1.98	GPa	5.3
K_x	Wing-Tail spring	0.5, 2.0	1.0×10^8	1.10×10^8	$\frac{N}{m}$	10.3
K_y	Wing-Tail spring	0.5, 2.0	1.0×10^8	1.12×10^8	$\frac{N}{m}$	11.8
K_z	Wing-Tail spring	0.5, 2.0	1.0×10^8	1.13×10^8	$\frac{N}{m}$	13.1
M_x	Wing-Tail spring	0.5, 2.0	1.0×10^8	1.09×10^8	$\frac{Nm}{rad}$	9.4
M_y	Wing-Tail spring	0.5, 2.0	1.0×10^8	1.02×10^8	$\frac{Nm}{rad}$	2.0
M_z	Wing-Tail spring	0.5, 2.0	1.0×10^8	1.09×10^8	$\frac{Nm}{rad}$	8.9

4.2.3 FEM Updating Results

The resonance modes that are identified most clearly in the GVT are the first seven structural modes of the X-HALE. These are the first five out-of-plane bending modes and the first two torsion-in-plane coupled modes. These modes were used in the FEM updating process and the outcome of the update is presented and discussed here. The rigid body plunge mode coming from the spring-based suspension set up in the laboratory was identified using DC accelerometers. Interestingly, the regular vibration accelerometers also resolved the sub 0.5 Hz plunge mode, but the noise levels were an order of magnitude higher than the accelerations read by

the DC accelerometers. This highlighted the value of the DC accelerometer in such a GVT (described further in Section 4.3).

From the design variables presented in Table 2, it can be observed that the updated FEM has different values of stiffnesses for the different wing sections and joiners. This is expected because there is no uniformity in the wings and/or joiners in the as-built structure. The uncertainties in the actual structure are reflected in the spread of the material properties in the updated FEM. The natural frequencies of the X-HALE before and after updating the FEM, and compared to the GVT conducted in the laboratory are provided in Tables 3 and 4 for the outboard and inboard configurations, respectively. As noted above, the FEM updating was conducted considering both configurations simultaneously. The errors between both inboard and outboard configurations compared to the experimental GVT data are highlighted in Fig. 11, indicating that the first seven computational elastic modes match the experimental under 2% error.

The FEM updating was conducted considering both the configurations (inboard and outboard) simultaneously. The errors between both configurations compared to the experimental GVT data are highlighted in Fig. 11, indicating that after the FEM updating, the first seven FEM elastic modes match the experimental results under 2% error.
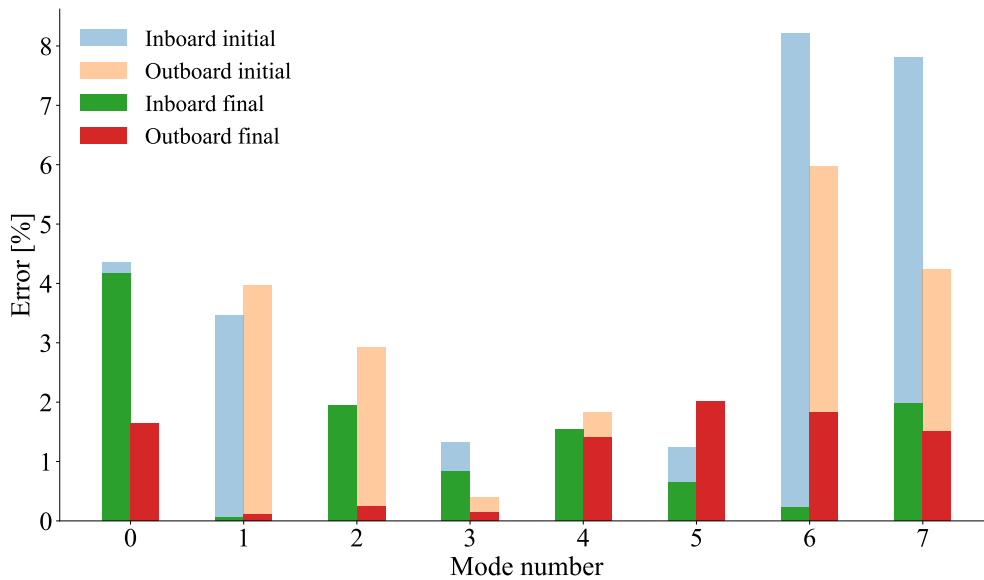

Figure 11: Percent error after updating using GVT results compared to the initial FEM of the X-HALE for the inboard and outboard configurations. Mode 0 is the plunge mode related to the suspension.

Table 3: Results of FEM updating for the X-HALE: outboard configuration.

		Laboratory GVT	Initial FEM		Updated FEM	
Mode #	Mode type	Frequency (Hz)	Frequency (Hz)	Difference (vs. GVT) %	Frequency (Hz)	Difference (vs. GVT) %
0	Plunge	0.28	0.27	−4.3	0.27	−4.2
1	1 OOP	0.99	0.96	−3.5	0.99	0.1
2	2 OOP	2.74	2.76	0.6	2.69	−1.9
3	1 T/2 IP	4.24	4.30	1.3	4.28	0.8
4	3 OOP	4.53	4.60	1.5	4.46	−1.5
5	2 T/3 IP	6.23	6.15	−1.2	6.27	0.7
6	4 OOP	7.18	7.77	8.2	7.20	0.2
7	5 OOP	8.10	8.73	7.8	8.26	2.0

Another interesting takeaway is that the different configurations (inboard or outboard) yield different reductions in percent errors. The in-plane bending and torsional modes show the

Table 4: Results of FEM updating for the X-HALE: inboard configuration.

		Laboratory GVT	Initial FEM		Updated FEM	
Mode #	Mode type	Frequency (Hz)	Frequency (Hz)	Difference (vs. GVT) %	Frequency (Hz)	Difference (vs. GVT) %
0	Plunge	0.28	0.28	−1.7	0.28	−1.7
1	1 OOP	0.95	0.91	−4.0	0.95	−0.1
2	2 OOP	2.70	2.78	2.9	2.71	0.2
3	1 T/2 IP	4.75	4.77	0.4	4.76	0.1
4	3 OOP	4.50	4.58	1.8	4.44	−1.4
5	2 T/3 IP	6.90	7.03	1.8	7.04	2.0
6	4 OOP	7.35	7.79	6.0	7.22	−1.8
7	5 OOP	8.38	8.74	4.2	8.26	−1.5

largest difference between the two configurations, while the out-of-plane bending modes remain similar between the differently deformed configurations. Figure 12 shows the reduction in error between the initial and final FEM for both the configurations.
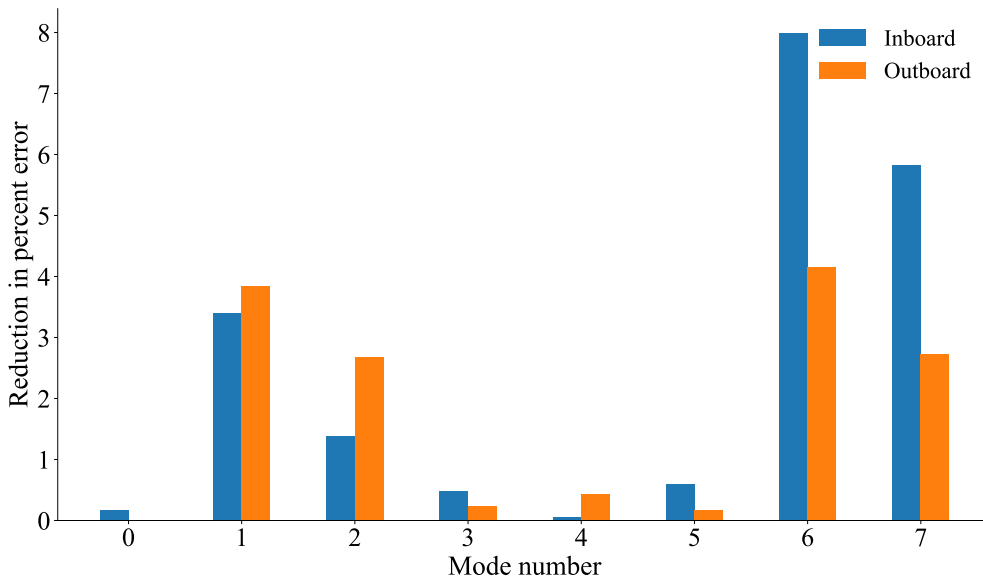

Figure 12: Reduction in percent error after calibration using GVT results compared to the initial FEM of the X-HALE for the inboard and outboard configurations.

4.3 Validation of GVT and FEM Updating Methodologies

As part of characterizing the very flexible structure and validating the methodologies both for conducting GVT and updating its FEM, a free-free GVT was conducted on the X-HALE. The objective is to identify true free-free modal parameters of the VFA by eliminating the effect of the support and getting as close as possible to the one order of magnitude separation between the suspension related modes and the fundamental elastic mode of the structure. Note that this step would not be practical to most VFA at large scale, but it is introduced here to validate the new methodology that includes the effect of the suspension system as used above.

In order to capture low-frequency vibrations, DC accelerometers (which are DC-coupled), and can respond down to zero Hertz were used. They can be used to measure static, as well as dynamic acceleration. In order to minimize the influence of the support, the aircraft needs to be connected to a suspension system that offers an order of magnitude of separation between the suspension related rigid body modes and the elastic modes of the aircraft. To accomplish this separation, a suspension setup made of 75-ft long, low-stiffness bungee cords that would sustain the weight of the aircraft and remain in the linear region of deformation was designed.

The X-HALE was suspended from a crane bucket that was connected to the airframe using two bungee cords. The crane, X-HALE, bungee cords, and various components used to create the soft suspension to approximate the free-flying conditions are shown in Fig. 13.
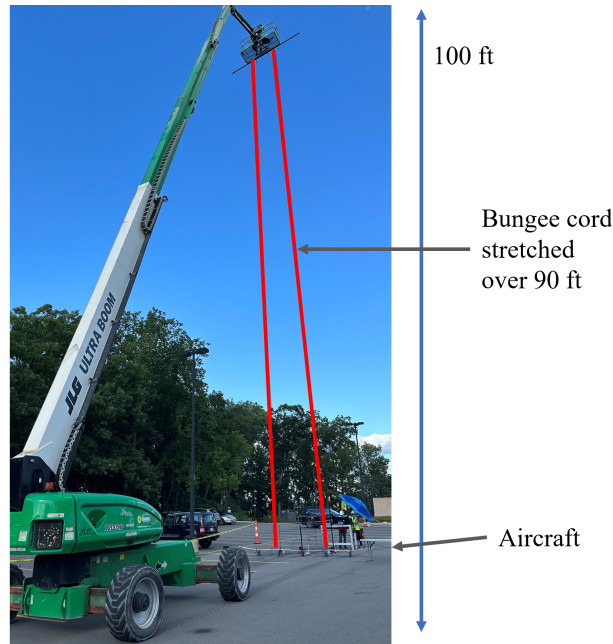

Figure 13: The crane with the X-HALE suspended from it using bungee cords during the free-free GVT.

The results of the free-free GVT on the X-HALE, and the comparisons with the predicted data from the updated FEM are summarized in Table 5, indicating a good match for the plunge and the roll modes of the aircraft, and very good matching of the first few elastic modes.

Table 5: Results of the X-HALE free-free GVT compared with updated FEM.

		Frequency (Hz)				Difference (%)	
		Updated FEM		GVT		Predicted Num. vs Exp.	
Mode #	Mode type	Inboard	Outboard	Inboard	Outboard	Inboard	Outboard
0	Plunge	0.17	0.18	0.21	0.20	−18.0	−9.1
0	Roll	0.18	0.32	0.22	0.31	−19.2	2.5
1	1 OOP	0.94	0.97	0.95	0.98	−0.8	−0.6
2	2 OOP	2.69	2.69	2.71	2.67	−0.8	0.5
3	1 T/ 2 IP	4.76	4.28	–	4.22	–	1.3
4	3 OOP	4.43	4.46	4.49	4.46	−1.3	0.0
5	2 T/3 IP	7.04	6.27	7.04	6.36	0.0	−1.5
6	4 OOP	7.22	7.19	7.43	7.32	−2.9	−1.8
7	5 OOP	8.25	8.26	8.38	8.44	−1.5	−2.3

5 CONCLUDING REMARKS

This paper presented the FEM updating after GVT for a very flexible aircraft exhibiting large deformations under self-weight in different suspension configurations. For a VFA, it may not be practical or feasible to create a suspension that allows an order of magnitude separation between the rigid body modes and the fundamental elastic mode of the structure. This requires accounting for the suspension both during the GVT and in the subsequent FEM updating. This can be achieved by characterizing the suspension upfront as an isolated component, and adding

the suspension characteristics in the FEM of the VFA. The GVT of the X-HALE followed the methodology described above and was successfully able to characterize and model the suspension dynamics for the multiple degree of freedom suspension setup.

Since a VFA undergoes large deflections in its flight regime, the linear, unloaded, and undeformed shape is not sufficient to capture the various nonlinearities exhibited by the structure within its operating conditions. The different deformed shapes change the stiffness characteristics of the structure. Large displacements cause local variations in the skin and other stiffening elements present in the wings. The FEM updating methodology applied to the X-HALE was modified to account for uncertainties that come from the presence of the various components used in its construction. The FEM update process applied to the X-HALE was performed using the suspension setup from the laboratory GVT, and after updating the FEM in the presence of the laboratory suspension, the springs were removed from the FEM. This FEM was used to create a prediction for a free-free GVT performed on the X-HALE, and validated by the results of the free-free GVT.

This work demonstrated that by properly characterizing the suspension and structure in a practical laboratory setting, with a suspension mechanism that does not provide the desired order of magnitude separation between the rigid body and elastic modes, enough information can be recovered to characterize the VFA structure. The FEM updating methodology, which allows multiple shapes with large deformations to be simultaneously considered, was applied to update the X-HALE FEM, and even with sources of uncertainty, the updated FEM was able to match the experimental results of the X-HALE within 2% error for the first seven modes. This is promising, and the results highlight the ability of the GVT and FEM updating methodology to sufficiently capture the structural dynamics behavior of the VFA.

6 REFERENCES

[1] Peeters, B., Debille, J., and Climent, H. (2008). Modern solutions for ground vibration testing of small, medium and large aircraft. *SAE International Journal of Aerospace*, 1(1), 732–742. doi:10.4271/2008-01-2270.

[2] Göge, D., Lubrina, P., Böswald, M., et al. (2007). Ground Vibration Testing of Large Aircraft - State-of-the-Art and Future Perspectives. In *Proceedings of IMAC XXV*. Orlando, FL.

[3] Lo, W., Shih, C., and Hinote, G. (2001). Ground Vibration Test of a Commercial Aircraft. In *Proceedings of SPIE*, vol. 4359. Society of Photo-Optical Instrumentation Engineers, pp. 92–97.

[4] Pickrel, C. R., Foss, G. C., Phillips, A., et al. (2006). New Concepts in Aircraft Ground Vibration Testing. *Sound and Vibration*, 40, 12–18.

[5] Xie, C., Liu, Y., Yang, C., et al. (2016). Geometrically Nonlinear Aeroelastic Stability Analysis and Wind Tunnel Test Validation of a Very Flexible Wing. *Shock and Vibration*, 2016, 1–17. doi:10.1155/2016/5090719.

[6] van Schoor, M. and von Flotow, A. (1990). Aeroelastic Characteristics of a Highly Flexible Aircraft. *Journal of Aircraft*, 27(10), 901–908. doi:10.2514/3.45955.

[7] Kehoe, M. W. (1987). Aircraft Ground Vibration Testing at NASA Ames-Dryden Flight Research Facility. Tech. rep., NASA TM-88272.

[8] Böswald, M., Vollan, A., Govers, Y., et al. (2011). Solar Impulse - Ground Vibration Testing and Finite Element Model Validation of a Lightweight Aircraft. In *Proceedings of IFASD 2011*. Paris, France.

[9] Woehrle, T. G., Costerus, B. W., and Lee, C. L. (1995). Modal Analysis of PATHFINDER Unmanned Air Vehicle. In *Proceedings of IMAC XIII*. Nashville, TN.

[10] Charmbalis, G. and Cooper, J. (2013). Vibration Testing of Aeroelastic Structures Containing Geometric Stiffness Nonlinearities. In *54th AIAA/ASME/ASCE/AHS/ASC Structures, Structural Dynamics, and Materials Conference*. Boston, MA: AIAA. doi:10.2514/6.2013-1561.

[11] Chang, C.-S., Hodges, D., and Patil, M. (2008). Flight Dynamics of Highly Flexible Aircraft. *Journal of Aircraft*, 45(2), 538–545. doi:10.2514/1.30890.

[12] Jones, J. and Cesnik, C. E. S. (2015). Preliminary Flight Test Correlations of the X-HALE Aeroelastic Experiment. *Aeronautical Journal of The Royal Aeronautical Society*, 119(1217), 855–870. doi:10.1017/S0001924000010952.

[13] Sharqi, B. and Cesnik, C. E. S. (2020). Ground Vibration Testing on Very Flexible Aircraft. In *AIAA Scitech Forum*. Orlando, FL. doi:https://doi.org/10.2514/6.2020-1902.

[14] Sharqi, B. and Cesnik, C. E. S. (2023). Finite Element Model Updating for Very Flexible Wings. *Journal of Aircraft*, 60(2), 476–489. doi:https://doi.org/10.2514/1.C036894.

[15] Chang, C.-S. and Hodges, D. (2007). Parametric Studies on Ground Vibration Test Modeling for Highly Flexible Aircraft. *Journal of Aircraft*, 44(6), 2049–2059. doi:10.2514/1.30733.

[16] Masri, S. and K. Caughey, T. (1979). A Nonparametric Identification Technique for Nonlinear Dynamic Problems. *Journal of Applied Mechanics*, 46(2), 433–447. doi:10.1115/1.3424568.

[17] Böswald, M., Govers, Y., Vollan, A., et al. (2010). Solar Impulse – How to Validate the Numerical Model of a Superlight Aircraft with A340 Dimensions! In *Proceedings ISMA 2010*. Leuven, Belgium.

[18] Ereiz, S., Duvnjak, I., and Fernando Jiménez-Alonso, J. (2022). Review of Finite Element Model Updating Methods for Structural Applications. *Structures*, 41, 684–723. ISSN 23520124. doi:https://doi.org/10.1016/j.istruc.2022.05.041.

[19] Li, D. and Zhang, J. (2023). Finite Element Model Updating Through Derivative-Free Optimization Algorithm. *Mechanical Systems and Signal Processing*, 185. ISSN 10961216. doi:https://doi.org/10.1016/j.ymssp.2022.109726.

[20] Cesnik, C. E. S., Senatore, P. J., Su, W., et al. (2012). X-HALE: A Very Flexible Unmanned Aerial Vehicle for Nonlinear Aeroelastic Tests. *AIAA Journal*, 50(12), 2820–2833. ISSN 00011452. doi:https://doi.org/10.2514/1.J051392.

[21] Sharqi, B. and Cesnik, C. E. S. (2024). Finite Element Model Updating of a 3D Printed Swept Wing. In *AIAA SCITECH 2024 Forum*. Orlando, FL. doi:https://doi.org/10.2514/6.2024-1730.

[22] Pastor, M., Binda, M., and Harčarik, T. (2012). Modal Assurance Criterion. *Procedia Engineering*, 48, 543–548. ISSN 1877-7058. doi:https://doi.org/10.1016/j.proeng.2012.09.551.

COPYRIGHT STATEMENT